Int. J. Electrochem. Sci., 7 **(2012)** 1840 - 1851

International Journal of ELECTROCHEMICAL SCIENCE
www.electrochemsci.org

Cyclic Calcium Phosphate Electrodeposition on Porous Silicon

J. Hernández-Montelongo[*], *A. Muñoz-Noval, V. Torres-Costa, R.J. Martín-Palma, M. Manso-Silvan*

Departamento de Física Aplicada, Universidad Autónoma de Madrid, 28049. Madrid, Spain.
[*]E-mail: jacobo.hernandez@uam.es

Received: 25 August 2011 / *Accepted:* 13 February 2012 / *Published:* 1 March 2012

Calcium phosphate (CaP) on porous silicon (PSi) has been proposed to generate composite bioceramics for osseous tissue regeneration. Usually, CaPs prepared by biomimetic and electrochemical methods stem from a single aqueous solution. We propose herein a diversified method that consists on independent calcium (Ca) and phosphate (P) electrodeposition cycles. In this way, the PSi layer is sequentially immersed in the Ca-P solutions, and the electrical current reversed in accordance, allowing both species to react on the porous matrix during a given number of cycles. The main advantage of our proposed method is that the individual variables of each step can be controlled and studied independently. That means that the main electrodeposition parameters such as pH, current density and reaction time can be adjusted independently for Ca and P solutions. The characterization by SEM, FTIR, XRD and EDX demonstrates that, for selected conditions, our proposed method allows depositing a hydroxyapatite layer on PSi.

Keywords: porous silicon, calcium phosphate, hydroxyapatite, cyclic electrodeposition

1. INTRODUCTION

Porous silicon (PSi), which consists of silicon nanocrystals embedded in a porous amorphous matrix, is an excellent biomaterial given its biocompatibility, biodegradability and bioresorbability. It has been successfully used in drug delivery, biosensing, and tissue engineering applications [1-3]. As an electroactive porous material, PSi can be used as a matrix for the deposition of a wide range of different materials like metals and conducting polymers following electrochemical processes [4-7]. Since hydroxyapatite ($Ca_{10}(PO_4)_6(OH)_2$, HAP) and derived substituted compounds constitute the inorganic part of natural bone [8], calcium phosphate (CaP) coatings on PSi have been proposed as cellular scaffolds for osseous tissue regeneration [9-12]. There are different techniques to produce CaP coatings [13-16] including plasma spraying, sputtering, laser ablation, sol-gel processes,

electrodepostion or biomimmetic growth. However, only sol-gel processes, electrodepostion and biomimmetic growth have been reported for the deposition of CaP on PSi [11, 12, 17]. Usually, electrochemical methods utilize simulated body fluids (SBF) or CaP aqueous solutions under a cathodic current [8, 12, 14, 17-19].

Since CaP is an ionic compound, in this work we propose an alternative electrochemical process that consists on synthesizing CaP by deposition of Ca and P on subsequent cycles. Although the final structural state of the materials differs notably, the principle behind this process is similar to that of electrochemical atomic layer epitaxy (ECALE), a technique used to produce semiconductor deposits under ambient pressure and temperature [20]. In this way, the PSi layer is alternately immersed in Ca and P solutions, and the applied electrodeposition current reversed in accordance, allowing both species to react on the porous matrix between cycles. The main advantage of this method is that the individual variables of each step such as pH, current density and reaction time, can be controlled and studied independently [20-22]. In that sense, the objective of this work is to describe and to explain the CaP synthesis on PSi by a cyclic method, as well as to show that by controlling the individual variables of each step, in Ca and P solutions, it is possible to direct the synthesis towards specific CaP phases.

2. EXPERIMENTAL

2.1. Sample preparation

PSi was fabricated by electrochemical etching p^+ type silicon (boron-doped, orientation <100>, resistivity of 0.01-0.02 Ωcm) wafers in HF (48%):EtOH (1:2) solution. PSi layers of approximately 4 μm thickness and 60 % porosity are obtained by applying a constant current density of 50 mA/cm^2 for 90 s.

For cyclic electrodeposition process a Ca^{+2}:EtOH (2:1) solution (Ca^{+2} from $CaCl_2$ 0.1 M at pH = 5.5) and a HPO_4^{-2}:EtOH (2:1) solutions (HPO_4^{-2} from Na_3PO_4 0.1 M adjusted to pH = 7.2 with H_3PO_4) were used. The particular pH values were selected because an acid medium favours the presence of Ca^{+2} in Ca solutions [23] and PSi with medium porosity (60%) tolerates neutral pH values though it dissolves in basic media [24]. The PSi layer was alternately immersed in the Ca and P solutions under the following standard conditions: 1 mA/cm^2 of cathodic current density in Ca solution and 1 mA/cm^2 of anodic current density in P solution, during 30 s controlled by a potentiostat (EG&G Princeton Applied Research). PSi was rinsed in ethanol between each step and 20 Ca/P cycles were made in total. Also CaP was synthesized at different ratios of Ca/P current densities (I_{Ca}/I_P = 1, 1.67, 2). Additional experiments were performed under different ratios of Ca/P reaction times (t_{Ca}/t_P = 1, 1.67, 2). All reactions were carried out with fresh Ca-P solutions at room temperature but a thermal post-annealing at 800 °C for an hour was applied to enhance crystallinity of particular samples.

2.2. Characterization

The morphology of the CaP particles on PSi was determined by scanning electron microscopy (SEM) at 20 kV detecting secondary electrons (Hitachi S-3000N). The Ca/P atomic ratio was

estimated by energy-dispersive X-ray analysis (EDX) with an INCA X-sight from Oxford Instruments within the SEM equipment. The resistance increment of the global system during electrodepostion was obtained from voltage-time characteristics measured at constant current in the potentiostat. The chemistry of the CaP/PSi samples was analyzed by Fourier transformed infrared spectroscopy (FTIR) in specular reflection mode using a Brücker mod. IFS 60v (4 cm^{-1} resolution, 7000-550 cm^{-1} range) and by X-ray diffraction (XRD) using a Siemens D5000 diffractometer working in grazing incidence mode by fixed incidence angle at 0.5º. The XRD analysis was performed from θ = 10º to θ = 60º degrees with an angle increment of $\Delta\theta$ = 0.04º and eight seconds between measurements.

3. RESULTS AND DISCUSSION

In order to confirm the feasibility of CaP films by the proposed process, a series of samples were prepared with increasing number of alternating cycles. Fig. 1 shows that the process generates a heterogeneous deposition.

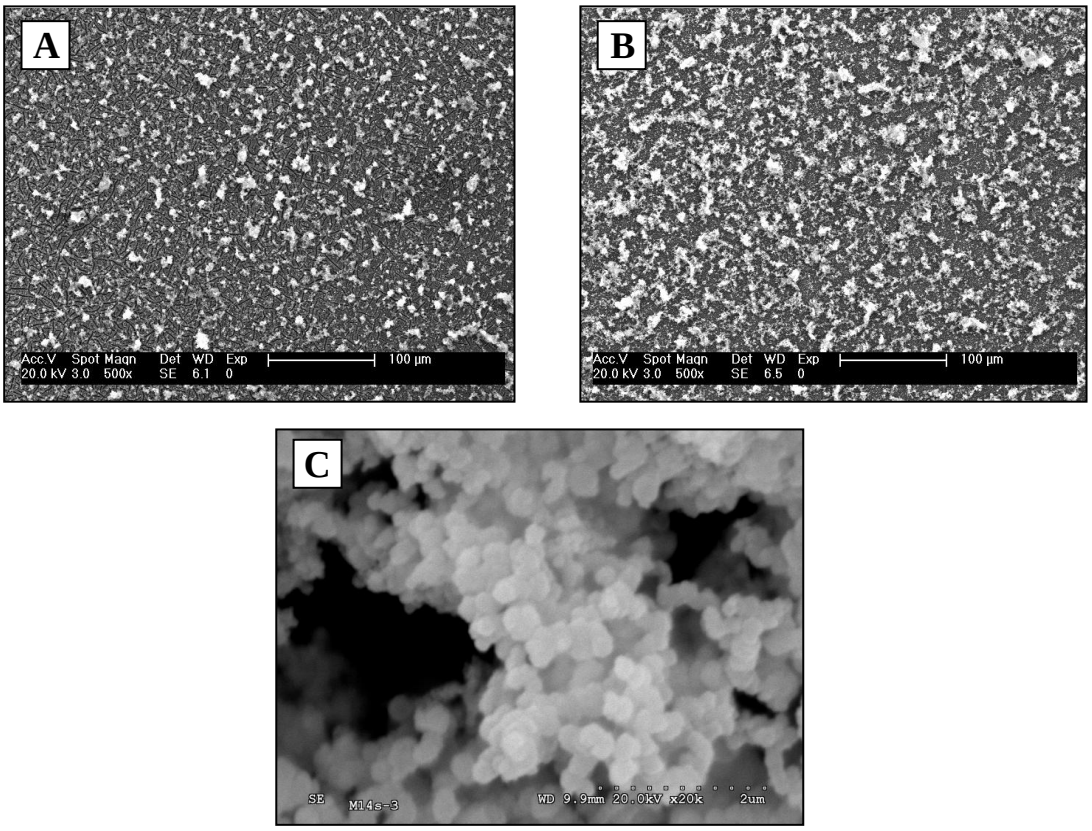

Figure 1. SEM images of CaP on PSi reacted under standard conditions: a) at 5th cycle, b) at 20th cycle and c) higher magnification of CaP particles reacted at 20th cycle.

The heterogeneous nucleation induced is similar to that obtained [18] in an electrodeposition process on Ti_6Al_4V using combined Ca-P aqueous solutions under a cathodic current. Basically, it

consists of small surface islands reaching some tens of micrometers. Favoured sites of nucleation are given by the surface roughness, which is enhanced in our case by the presence of PSi. With increasing reaction time, or number of cycles in our case, island density and size increase as illustrated in the SEM images corresponding to the 5th and 20th cycles (Fig. 1A & 1B, respectively). Higher magnification image was obtained to dig-out in the internal microstructure of the grown islands (Fig. 2C). This SEM image shows that the CaP particles are spherical, around 300 nm in diameter and they are agglomerated in clusters. Morphologically, the CaP particles are similar to others synthesized previously [25], although this particular shape was obtained in an aqueous precipitation method at pH = 9 following a sintering step at 950 ºC.

In order to provide a model for the growth of the CaP films we have evaluated the electrical parameters in the cell. The electrochemical system can be approximated to a model consisting of a resistance and a capacitor connected in series. For an RC circuit under direct current, the potential is given by [26]:

$$V = iR + \frac{i}{C}\int dt \qquad (1)$$

where V is the applied potential; i, the current; R, the resistance; C, the capacitance and t is time. Fig. 2 shows the experimental V vs t curves corresponding to the 5th and 20th cycles of Ca and P deposition (i.e. last deposition steps of samples in figures 1A and 1B, respectively). The asymptotic saturation of V to a constant value suggests that the $1/C$ term in (1) is negligible, which can be attributed to the high capacitance associated with the large internal surface of PSi [27-30].

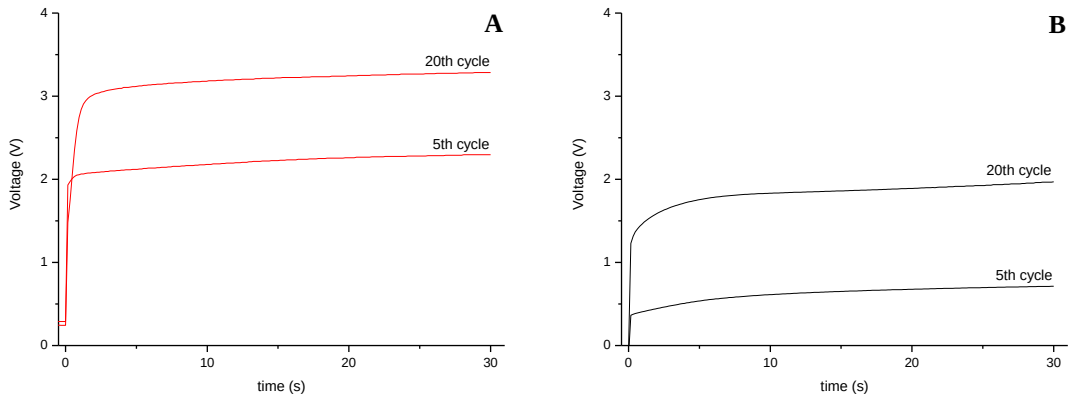

Figure 2. V vs t curves for the 5th and 20th cycles: a) corresponding to Ca solution (cathodic current) and b) corresponding to P solution (anodic current).

The constant value of V for a fixed electrodeposition current (1 mA/cm^2, cathodic current for Ca solution and anodic current for P solution), allows the determination of an effective resistance value for each electrodeposition step by applying Ohm's law. The plot in Fig. 3 shows that this effective resistance increases linearly with the number of cycles suggesting that CaP growth in PSi is also linear

with the number of cycles. However, it is possible that the resistance increase has some contribution from oxide formation in the PSi matrix, as a consequence of the voltage reached during the process [31]; 3.3 V in Ca solution and 2 V in P solution.

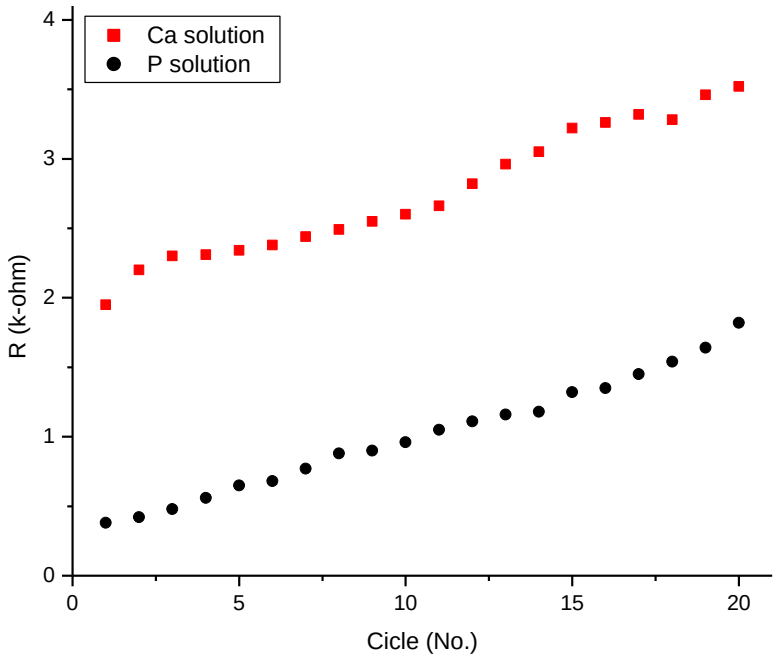

Figure 3. Resistance increment with cycles for the independent Ca and P solutions.

Fig. 4 shows the FTIR spectra in specular reflection mode for a fresh PSi layer and a CaP coating on PSi. The PSi spectrum shows relatively strong interference fringes, which is typical of PSi layers [29, 32]. Also, characteristic silicon-hydrogen bonds of nanostructured PSi are identified at 2116, 906, 661 and 624 cm^{-1} [1, 29]. In the case of the CaP/PSi spectrum, the fringes fade because of infrared absorption by CaP surface clusters. PO_4 ν_3 peaks are observed at 1091, 1042, 962 cm^{-1}, which are related to HAP [18, 33]; as well as the signal in 602 cm^{-1} of PO_4 ν_4 [33]. Additionally, absorption around 1455 cm^{-1} corresponding to CO_3 ν_3 is identified [33]. This carbonate peak is probably originated from the reaction of hydroxyl ions with carbon dioxide ($CO_2 + 2OH^- \leftrightarrow CO_3^{-2} + H_2O$) [18].

After the initial evidences of feasibility of CaP coatings by the proposed cyclic process, we devoted our efforts to the control of the coating composition and structure by varying process parameters such as the current and time applied in each one of the reactive Ca and P electrolytes.

Diffraction studies were performed in order to extract information relative to the crystalline structure of the CaP deposits. Fig. 5 shows XRD diagrams in grazing incidence mode at different ratios of Ca/P electrodeposition current densities (I_{Ca}/I_P = 1, 1.67, 2). In the experiment of I_{Ca}/I_P = 1, main 2θ values corresponding to HAP [8, 13, 34] are well identified with a trace of monotite ($CaHPO_4$). On the other hand, for the cases of I_{Ca}/I_P = 1.67 and 2, traces of monotite and brushite ($CaHPO_4 \cdot 2H_2O$) are notorious within a dominant HAP structure too.

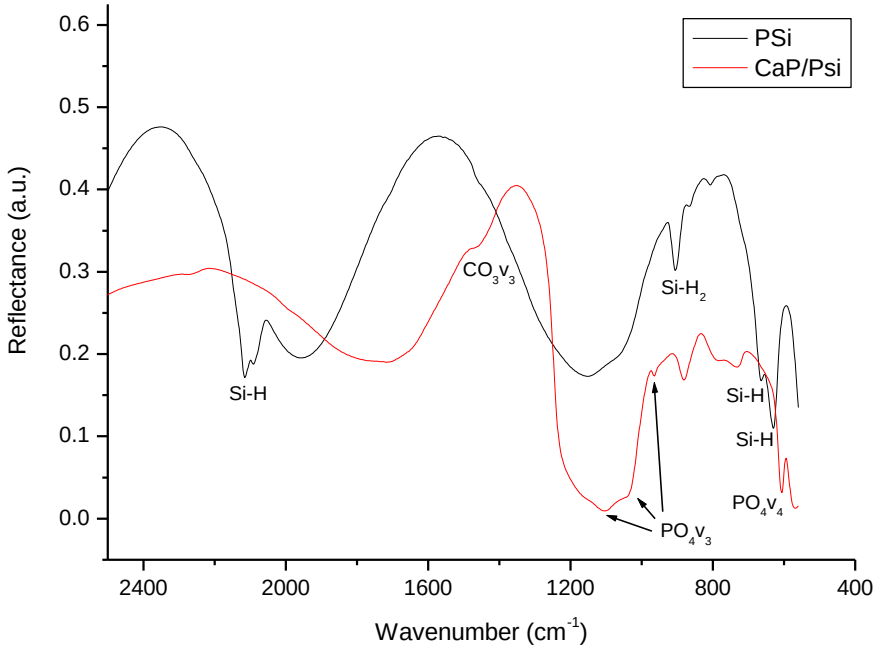

Figure 4. FTIR spectra of PSi and CaP/PSi samples made under standard conditions

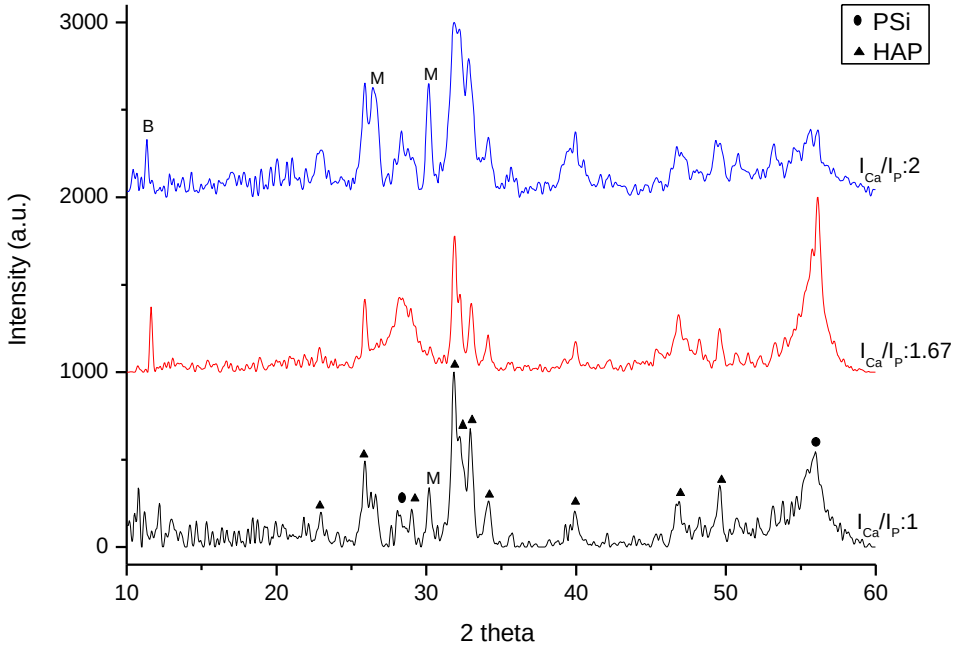

Figure 5. XRD diagrams at different ratios of Ca/P current densities (I_{Ca}/I_P = 1, 1.67, 2) for a t_{Ca}/t_P =1. M = Monotite, B = Brushite.

Fig. 6 shows XRD diagrams on grazing incidence mode at different ratios of Ca/P reaction times (t_{Ca}/t_P = 1, 1.67, 2). The main phases identified in the difractograms are the same as those found in the previous experiments. The more important difference is the lower crystallinity of HAP for t_{Ca}/t_P

= 1.67 and 2. The t_{Ca}/t_P = 1.67 diffractogram indicates a relatively strong presence of brushite in HAP and the t_{Ca}/t_P = 2 shows a solid solution of monotite-brushite traces in HAP. The relative increase of brushite and monotite phases creates a competitive environment for crystal growth that could not only affect to the quantity of HAP formed but also to the quality of the HAP crystals formed as suggested by the increase of the width at half maximum of the peaks attributed to HAP .

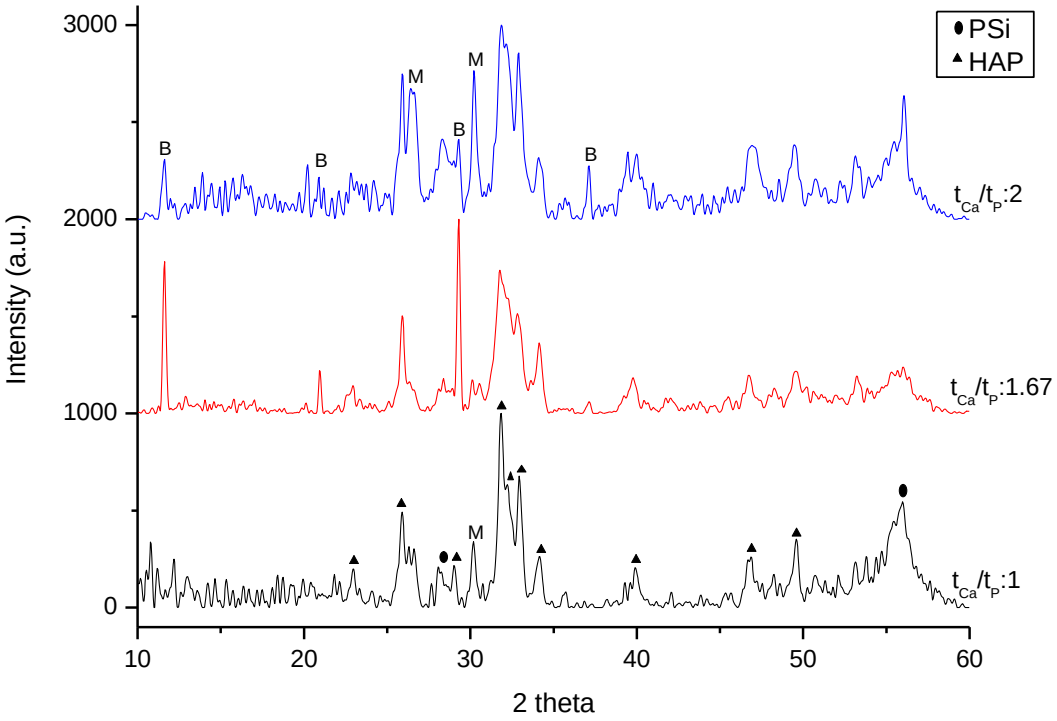

Figure 6. XRD diagrams at different ratios of Ca/P reaction times (t_{Ca}/t_P = 1, 1.67, 2) for a I_{Ca}/I_P = 1. M = Monotite, B = Brushite.

Estimation of the Ca/P atomic quantification from CaP clusters was done by EDX semiquantitative analysis. Graph in Fig. 7 shows the Ca/P atomic ratios for both experimental series (I_{Ca}/I_P and t_{Ca}/t_P). EDX allows observing the tendency of the Ca/P atomic ratios generated by the changes in electrodeposition conditions. The EDX measurements for I_{Ca}/I_P = 1 and t_{Ca}/t_P = 1, the Ca/P average atomic ratio was 1.63, close to the value of 1.67 corresponding to HAP [35-37]. On the other hand, in the other two ratios (1.67 and 2) in both experimental series, the Ca/P value decreased considerably. The reduction of Ca/P in these parameters ratios suggests the formation of other CaP phases in addition to HAP. The monotite and brushite detected by DRX in that experiments (Fig. 5 and 6) match very well because their respective Ca/P atomic ratio is 1 [38] reducing the ideal value of 1.67 corresponding to HAP.

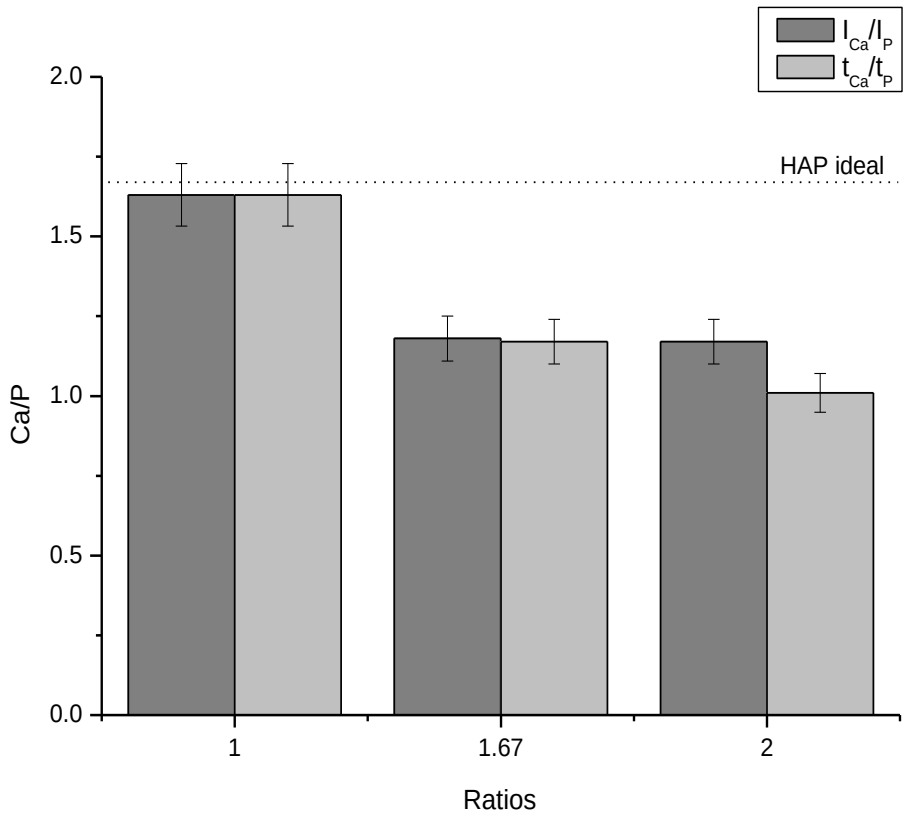

Figure 7. Ca/P atomic ratios for the films electrodeposited by different I and t ratios as determined by EDX.

From the evidences provided by the different techniques it is possible to provide an electrochemical mechanism for the growth of CaP on PSi. The process of cyclic activation of Ca and P deposition onto PSi, taking into account the respective polarity of the independent Ca and P solutions, is explained as a series of reduction-oxidation reactions. The presence of monotite and brushite traces in HAP suggests the following series of electrochemical reactions. At pH = 7.2 the phosphate ion is in the monohydrated form HPO_4^{-2} [26] and since the reduction potential of Ca^{+2} ion to metallic Ca is not reached (-2.8 V) [26] until the 10th cycle, in the first 10 cycles there is only a chemical formation of monotite and brushite given by [39, 40]:

$$Ca^{+2} + HPO_4^{-2} \rightarrow CaHPO_4 \quad (2)$$

$$Ca^{+2} + HPO_4^{-2} + 2H_2O \rightarrow CaHPO_4 \cdot 2H_2O \quad (3)$$

That means that, at the beginning, each respective current density in each solution works only as a force that move ions to PSi enhancing the chemical reaction on its surface. However, after the 10th cycle, in Ca solution there is a reduction from Ca^{+2} ion to metallic Ca as observed previously [7, 26]:

$$Ca^{+2} + 2e^- \rightarrow Ca \quad (4)$$

Then the metallic Ca is oxidized to monotite and brushite in the P solution as already suggested [39, 40], together with reactions 2 and 3:

$$Ca + HPO_4^{-2} \rightarrow CaHPO_4 + 2e^- \quad (5)$$

$$Ca + HPO_4^{-2} + 2H_2O \rightarrow CaHPO_4 \cdot 2H_2O + 2e^- \quad (6)$$

The OH^- ions are dominantly produced from reduction of water, although OH^- can also plausibly derive from ethanol dissolution and dissolved oxygen [41]:

$$2H_2O + 2e^- \rightarrow H_2 + 2OH^- \quad (7)$$

$$O_2 + 2H_2O + 4e^- \rightarrow 4OH^- \quad (8)$$

Thus, the monotite, brushite and metallic Ca react with OH^- resulting in the formation of HAP [19, 40-42]:

$$10CaHPO_4 + 12OH^- \rightarrow Ca_{10}(PO_4)_6(OH)_2 + 4PO_4^{-3} + 10H_2O \quad (9)$$

$$10CaHPO_4 \cdot 2H_2O + 12OH^- \rightarrow Ca_{10}(PO_4)_6(OH)_2 + 4PO_4^{-3} + 20H_2O \quad (10)$$

$$10Ca + 6PO_4^{-3} + 2OH^- \rightarrow Ca_{10}(PO_4)_6(OH)_2 + 20e^- \quad (11)$$

Due to the pH of the P solution, it is highly probable that most of the PO_4^{-3} reacts with water to produce HPO_4^{-2} [23] and the process restarts again in reactions 2 and 5. The reason of the monotite and brushite traces found when Ca/P ratios increase in I_{Ca}/I_P and t_{Ca}/t_P experiments may be the generation of an excess of metallic Ca. In fact, when PSi is reacting in the P solution at neutral pH, there are not enough HPO_4^{-2} and OH^- ions for all the metallic Ca generated. Consequently, some monotite and brushite formed can not react to produce HAP and nucleate on the substrate. It is patent that, for HAP formation, it is possible to avoid the formation of such phases by working in basic conditions [8, 43, 44].

The stability of the synthesized HAP at room temperature was confirmed with the thermal post-annealing at 800 °C made for an hour (Fig. 8). The XRD diffractogram of the annealed sample presents the same phases identified in the diffractogram obtained at room temperature. However, the annealing activates the crystalline structure as derived from the better definition of the diffractogram peaks. Besides, the 800 °C diffractogram presents other two main differences, the monotite peak at 30.2 is considerably reduced and the HAP peak at 32.2 shows an enhanced definition.

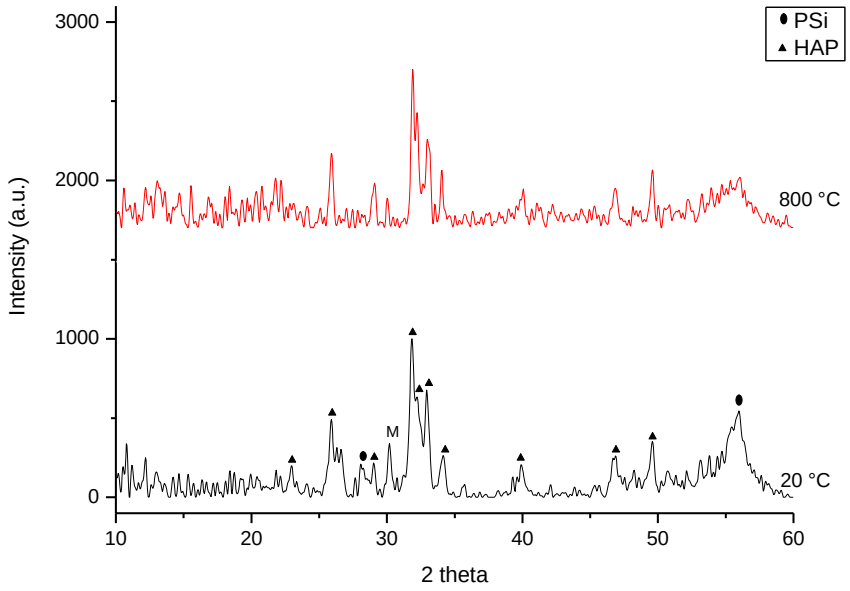

Figure 8. XRD diagrams at room temperature and after a thermal post-annealingat 800 °C of a film grown with $I_{Ca}/I_P = 1$ and $t_{Ca}/t_P = 1$. M = Monotite.

4. CONCLUSIONS

This work demonstrates that a method based on a cyclic electrodeposition in Ca and P electrolytes is suitable for the fabrication of CaP/PSi scaffolds and ceramics. CaP synthesis has been directed to HAP at room temperature by controlling parameters such as pH, current density and reaction time thinking on the formation of filling bioceramics with applications in bone tissue reconstruction. The process is liable to the growth of other phases with higher physiological solubility (monotite or brushite), which could be used for the production of drug delivery systems. On the other hand, an approximation to the mechanism of in situ CaP deposition was studied by a simple system resistance calculation. Finally, due to the flexibility of the method, it opens an alternative way of ionic compound synthesis on porous conductor substrates.

ACKNOWLEDGMENTS
This project was financed by Madrid Regional Grant “Microseres” and financial resources from Fundación Domingo Martínez. J. Hernández-Montelongo thanks the European Commission for his research grant from the program “Erasmus Mundus External Cooperation Windows Lot 20”.

References

1. R. J. Martin-Palma, M. Manso-Silvan and V. Torres-Costa, *J. Nanophotonics*, 4, 042502 (2010).
2. S. Dondapati and A. P. Sri, *Int J Pharm Pharm Sci.*, 1, 2 (2009).
3. M. P. Stewart and J. M. Buriak, *Adv Mater.*, 12, 12 (2000).

4. A.Munoz-Noval, V. Sanchez-Vaquero, V. Torres-Costa, D. Gallach, V. Ferro-Llanos, J. J. Serrano, M. Manso-Silvan, J. P. Garcia-Ruiz, F. del Pozo and R. J. Martin-Palma, *J.Biomed.Opt.*, 16, 2 (2011).
5. C. Renaux, V. Scheuren and D. Flandre, *Microelectronics Reliability.*, 40, 4-5 (2000).
6. J. D. Moreno, M. L. Marcos, F. Agulló-Rueda, R. Guerrero-Lemus, R. J. Martín-Palma, J. M. Martínez-Duart and J. González-Velasco, *Thin Solid Films.*, 348, 1-2 (1999).
7. M. Jeske, J. W. Schultze, M. Thönissen and H. Münder, *Thin Solid Films.*, 255, 1-2 (1995).
8. M. Manso, C. Jimenez, C. Morant, P. Herrero and J. M. Martinez-Duart, *Biomaterials.*, 21, 17 (2000).
9. W. Sun, J. E. Puzas, T. J. Sheu, X. Liu and P. M. Fauchet, *Adv Mater.*, 19, 7 (2007).
10. L. Pramatarova, E. Pecheva, D. Dimova-Malinovska, R. Pramatarova, U. Bismayer, T. Petrov and N. Minkovski, *Vacuum.*, 76, 2-3 (2004).
11. C. Shaoqiang, Z. Ziqiang, Z. Jianzhong, Z. Jian, S. Yanling, Y. Ke, W. Weiming, W. Xiaohua, F. Xiao and L. Laiqiang, *Appl.Surf.Sci.*, 230, 1-4 (2004).
12. L. T. Canham, C. L. Reeves, A. Loni, M. R. Houlton, J. P. Newey, A. J. Simons and T. I. Cox, *Thin Solid Films.*, 297, 1-2 (1997).
13. K. Rodríguez, S. Renneckar and P. Gatenholm, *ACS Appl. Mater. Interfaces.*, 3, 3 (2011).
14. P. Ballesteros, D. Yesid, H. A. Estupinan Duran and E. M. Cordoba Tutta, *Rev.fac.ing.univ.Antioquia.*, 54 (2010).
15. E. J. Anglin, L. Cheng, W. R. Freeman and M. J. Sailor, *Adv.Drug Deliv.Rev.*, 60, 11 (2008).
16. M. Manso, P. Herrero, M. Fernández, M. Langlet and J. M. Martínez-Duart, *J Biomed Mater Res-A.*, 64, 4 (2003).
17. L. T. Canham, J. P. Newey, C. L. Reeves, M. R. Houlton, A. Loni, A. J. Simons and T. I. Cox, *Adv Mater.*, 8, 10 (1996).
18. S. Rößler, A. Sewing, M. Stölzel, R. Born, D. Scharnweber, M. Dard and H. Worch, *J Biomed Mater Res-A.*, 64, 4 (2003).
19. C. Montero-Ocampo, D. Villegas and L. Veleva, *J.Electrochem.Soc.*, 152, 10 (2005).
20. B. W. Gregory and J. L. Stickney, *J. Electroanal. Chem.*, 300, 1-2 (1991).
21. V. C. Fernandes, E. Salvietti, F. Loglio, E. Lastraioli, M. Innocenti, L. H. Mascaro and M. L. Foresti, *J.Appl.Electrochem.*, 39, 11 (2009).
22. T. Torimoto, A. Obayashi, S. Kuwabata and H. Yoneyama, *Electrochem. Commun.*, 2, 5 (2000).
23. D. C. Harris, *Quantitative chemical analysis*, W.H. Freeman, New York (2003).
24. S. H. C. Anderson, H. Elliott, D. J. Wallis, L. T. Canham and J. J. Powell, *Phys. Stat. Sol. (a).*, 197, 2 (2003).
25. R. LeGeros, S. Lin, R. Rohanizadeh, D. Mijares and J. LeGeros, *J.Mater.Sci.Mater.Med.*, 14, 3 (2003).
26. A.J. Bard and L. R. Faulkner, *Electrochemical methods fundamentals and applications*, p. 833, John Wiley & Sons, New York (2001).
27. H. Föll, M. Christophersen, J. Carstensen and G. Hasse, *Mat. Sci. Eng. R.*, 39, 4 (2002).
28. V. Lehmann, *Electrochemistry of silicon*, Wiley Online Library (2002).
29. O. Bisi, S. Ossicini and L. Pavesi, *Surf. Sci. Rep.*, 38, 1-3 (2000).
30. V. Lehmann, W. Hönlein, H. Reisinger, A. Spitzer, H. Wendt and J. Willer, *Thin Solid Films.*, 276, 1-2 (1996).
31. F. Ronkel and J. W. Schultze, *J. Porous Mat.*, 7, 1 (2000).
32. V. Parkhutik, M. S. J. Martínez and E. G. Senent, *J. Porous Mat.*, 7, 1 (2000).
33. I.Rehman and W. Bonfield, *J.Mater.Sci.Mater.Med.*, 8, 1 (1997).
34. M. J. Arellano-Jiménez, R. García-García and J. Reyes-Gasga, *J. Phys. Chem. Solids.*, 70, 2 (2009).
35. E. Chadwick, O. Clarkin and D. Tanner, *J.Mater.Sci.*, 45, 23 (2010).

36. H. M. Kim, T. Himeno, M. Kawashita, T. Kokubo and T. Nakamura, *J. Roy. Soc. Interface.*, 1, 1 (2004).
37. S. Joschek, B. Nies, R. Krotz and A. Göpferich, *Biomaterials.*, 21, 16 (2000).
38. F. Driessens, M. Boltong, E. De Maeyer, R. Wenz, B. Nies and J. Planell, *Biomaterials.*, 23, 19 (2002).
39. A.Kar, K. S. Raja and M. Misra, *Surf. Coat. Tech.*, 201, 6 (2006).
40. L. Y. Huang, K. W. Xu and J. Lu, *J.Mater.Sci.Mater.Med.*, 11, 11 (2000).
41. X. Lu, Z. Zhao and Y. Leng, *J.Cryst.Growth.*, 284, 3-4 (2005).
42. J. Redepenning, T. Schlessinger, S. Burnham, L. Lippiello and J. Miyano, *J.Biomed.Mater.Res.*, 30, 3 (1996).
43. C. Lai, S. Q. Tang, Y. J. Wang and K. Wei, *Mater Lett.*, 59, 2-3 (2005).
44. A.Cuneyt Tas, F. Korkusuz, M. Timucin and N. Akkas, *J.Mater.Sci.Mater.Med.*, 8, 2 (1997)